Neurobiology of Disease

$Na_v1.1$ Localizes to Axons of Parvalbumin-Positive Inhibitory Interneurons: A Circuit Basis for Epileptic Seizures in Mice Carrying an *Scn1a* Gene Mutation

Ikuo Ogiwara,[1] Hiroyuki Miyamoto,[2] Noriyuki Morita,[3] Nafiseh Atapour,[2] Emi Mazaki,[1] Ikuyo Inoue,[1] Tamaki Takeuchi,[1] Shigeyoshi Itohara,[4] Yuchio Yanagawa,[6] Kunihiko Obata,[5] Teiichi Furuichi,[3] Takao K. Hensch,[2] and Kazuhiro Yamakawa[1]

Laboratories for [1]Neurogenetics, [2]Neuronal Circuit Development, [3]Molecular Neurogenesis, and [4]Behavior Genetics and [5]Neuronal Circuit Mechanisms Research Group, RIKEN Brain Science Institute, Wako, Saitama 351-0198, Japan, and [6]Department of Genetic and Behavioral Neuroscience, Gunma University Graduate School of Medicine and Solution-Oriented Research for Science and Technology, Japan Science and Technology Agency, Maebashi 371-8511, Japan

Loss-of-function mutations in human *SCN1A* gene encoding $Na_v1.1$ are associated with a severe epileptic disorder known as severe myoclonic epilepsy in infancy. Here, we generated and characterized a knock-in mouse line with a loss-of-function nonsense mutation in the *Scn1a* gene. Both homozygous and heterozygous knock-in mice developed epileptic seizures within the first postnatal month. Immunohistochemical analyses revealed that, in the developing neocortex, $Na_v1.1$ was clustered predominantly at the axon initial segments of parvalbumin-positive (PV) interneurons. In heterozygous knock-in mice, trains of evoked action potentials in these fast-spiking, inhibitory cells exhibited pronounced spike amplitude decrement late in the burst. Our data indicate that $Na_v1.1$ plays critical roles in the spike output from PV interneurons and, furthermore, that the specifically altered function of these inhibitory circuits may contribute to epileptic seizures in the mice.

Key words: SCN1A; $Na_v1.1$; severe myoclonic epilepsy in infancy; parvalbumin-positive; fast spiking; interneurons

Introduction

Voltage-gated sodium channels are essential for the generation and propagation of action potentials in electrically excitable tissues, such as brain, muscle, and heart. These channels are heteromultimeric protein complexes consisting of one α and one or two β subunits (Catterall, 2000). The pore-forming α subunits also serve as voltage sensors, whereas the accessory β subunits modulate the voltage dependence and kinetics and cellular localization of the α subunits. Four α and four β subunits have been identified in the mammalian brain.

The α type I sodium channel ($Na_v1.1$) has been reported to be expressed in the brain, in which it is localized to somata and dendrites of neurons (Westenbroek et al., 1989; Gong et al., 1999). To date, >100 heterozygous mutations of human *SCN1A* gene encoding $Na_v1.1$ have been reported in several human epileptic disorders, namely, generalized epilepsy with febrile seizure plus (GEFS+), intractable childhood epilepsy with generalized tonic-clonic seizures (ICEGTC), and severe myoclonic epilepsy in infancy (SMEI) (Escayg et al., 2000; Claes et al., 2001; Fujiwara et al., 2003). SMEI, or Dravet syndrome, is the most severe and intractable form of the *SCN1A*-associated epileptic disorders (Online Mendelian Inheritance in Man number 607208). SMEI begins in children under 1 year of age, who otherwise develop normally before disease onset. The first seizure is typically a unilateral or generalized tonic-clonic or clonic seizure often, but not always, associated with fever and is subsequently followed by additional generalized and partial seizures, ataxia, and mental decline. Because SMEI mutations are mainly heterozygous nonsense or frame-shift mutations leading to predicted loss of $Na_v1.1$ function, $Na_v1.1$ haploinsufficiency has been implicated in SMEI pathology (Sugawara et al., 2003; Meisler and Kearney, 2005; Mulley et al., 2005; Yamakawa, 2005).

Recently, Yu et al. (2006) generated $Na_v1.1$-null mice exhibiting spontaneous seizures and whole-cell sodium currents that were significantly reduced in isolated GABAergic interneurons but not in pyramidal cells from hippocampus, suggesting that loss of $Na_v1.1$ might specifically decrease inhibition resulting in epilepsy. However, a reexamination of $Na_v1.1$ distribution and localization in the brain is required to resolve why the loss of $Na_v1.1$ affects only inhibitory, but not pyramidal, neurons when both cell types express the channel.

Received Dec. 6, 2006; revised April 17, 2007; accepted April 18, 2007.

This work was supported in part by grants from RIKEN Brain Science Institute (I.O., K.Y.) and the Ministry of Education, Culture, Sports, Science, and Technology of Japan (I.O., Y.Y.). We thank the Research Resource Center at RIKEN Brain Science Institute for help in generating *Scn1a* knock-in mice and the rabbit anti-$Na_v1.1$ and -$Na_v1.6$ antibodies, DNA sequencing, and immunohistochemical analyses. We also thank Mr. Baljinder Singh for his comments and for editing and rewriting significant portions of this manuscript.

Correspondence should be addressed to Dr. Kazuhiro Yamakawa, Laboratory for Neurogenetics, RIKEN Brain Science Institute, 2-1 Hirosawa, Wako, Saitama 351-0198, Japan. E-mail: yamakawa@brain.riken.jp.

T. Takeuchi's present address: Neuroimmunology Research Group, Keio University School of Medicine, Tokyo 160-8582, Japan.

DOI:10.1523/JNEUROSCI.5270-06.2007

 0270-6474/07/275903-12$15.00/0

We report here the generation and characterization of knock-in mice carrying a truncation mutation in the *Scn1a* gene identical to the human SMEI mutation. We show the absence of truncated mutant $Na_v1.1$ in their brains, and the resultant $Na_v1.1$ haploinsufficiency causes epileptic seizures in these mice. Moreover, we describe a novel form of $Na_v1.1$ localization in the developing neocortex. $Na_v1.1$ is predominantly found at the axon initial segments of parvalbumin-positive (PV) interneurons. In the hippocampus, $Na_v1.1$ is also predominantly distributed within somata and axons of PV interneurons, whereas pyramidal neurons express $Na_v1.1$ at extremely low levels. Finally, we show that $Na_v1.1$ is involved in sustained high-frequency firing of neocortical fast-spiking interneurons. We propose that impaired function of the PV inhibitory circuit contributes to epileptic seizures in knock-in mice.

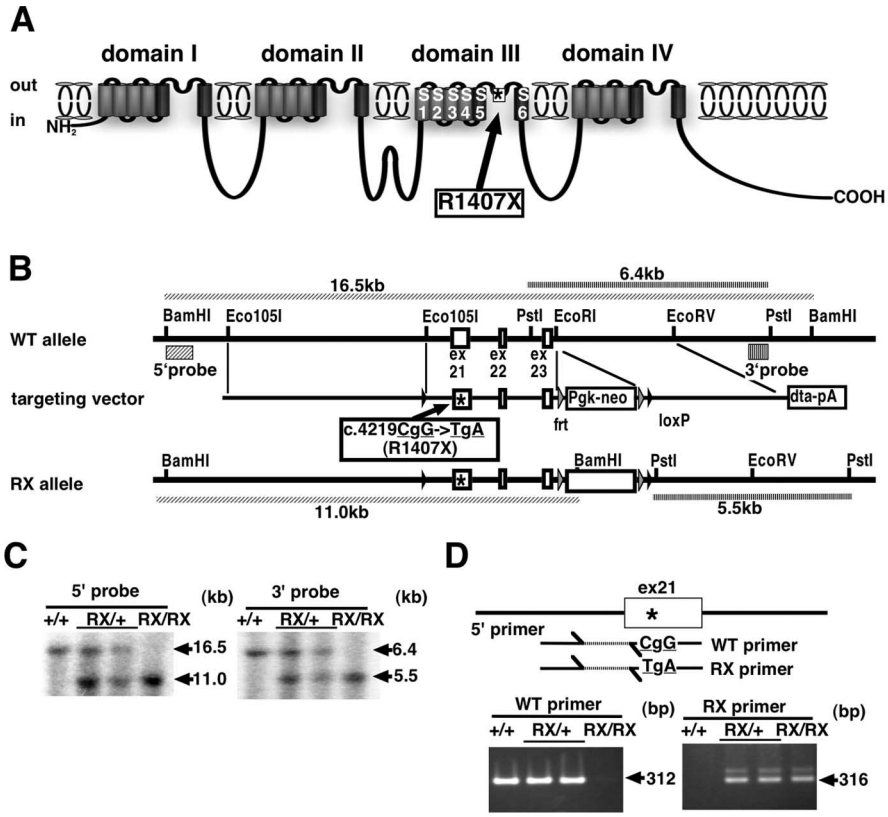

Figure 1. Generation of *Scn1a* knock-in mice with a nonsense mutation. ***A***, The RX nonsense mutation is located within a loop between segments 5 and 6 of domain III and could lead to production of truncated mutant $Na_v1.1$ missing the segment 6 of domain III, domain IV, and C terminus. The position of the RX mutation is represented by an asterisk. ***B***, Schematic representation of the wild-type *Scn1a* allele, the targeting vector, and the RX mutant *Scn1a* allele. The nucleotide substitution (CgG to TgA) in exon 21 leading to the RX mutation is represented by an asterisk. The *Bam*HI and *Pst*I sites, the probes used for Southern blot analysis, and the sizes of the restriction fragments detected by the probes are indicated. ***C***, Genotyping of offspring from heterozygote intercrosses by Southern blot analysis of *Bam*HI- or *Pst*I-digested mouse genomic DNA. ***D***, Verification of the presence of the RX mutation using PCR analysis of genomic DNA. The positions of primers and the sizes of PCR products are indicated. The position of the RX mutation is represented by an asterisk.

Materials and Methods

Mice were handled in accordance with the Animal Experiment Committee of RIKEN Brain Science Institute.

Construction of the targeting vector. We isolated a PAC clone 462C21 by screening a pooled mouse genomic PAC library (BACPAC Resource Center, Oakland, CA) with dot blot hybridization using [α-^{32}P] dCTP-labeled DNA that corresponded to the genomic fragment containing exon 21 of the *Scn1a* gene as the probe. A 5.0 kb *Eco*105I-*Hin*dIII fragment, a 6.0 kb *Eco*RI fragment, and a 4.0 kb *Pst*I-*Eco*RV fragment of the PAC clone were subcloned into pBluescript II SK(-) (Stratagene, La Jolla, CA) to obtain p462H105I, p462EI, and p462PEv, respectively. Next, using the QuikChange Site-Directed Mutagenesis kit (Stratagene), the *Eco*RI sites in p462H105I and p462PEv were inactivated, and the nucleotide substitution (CgG to TgA) leading to the R1407X (RX) mutation was introduced into p462EI. All constructs were verified by sequencing. A 6.0 kb *Eco*RI fragment of p462EI mutated was inserted into the *Eco*RI site of p462H105I mutated to yield p1-8-6(e), whose 9.0 kb *Apa*I-*Sma*I fragment was then inserted into ploxPfrtPGK-neofrt to generate pe-frt3. A 2.8 kb *Eco*RI-*Xho*I fragment of p462PEv mutated was inserted into *Eco*RI-*Xho*I sites of pBluescript II SK(-) to obtain pPEv2.8k, in which an *Xho*I-*Not*I-*Xho*I cassette was then inserted into the *Xho*I site, and the inactivated *Eco*RI site was restored using the QuikChange Site-Directed Mutagenesis kit. Subsequently, the *Not*I fragment of the resultant plasmid vector was inserted into the *Not*I site of pe-frt3 to generate pe-frt-Pm7. pe-frt-Pm7 was then digested with *Eco*105I and inserted with the loxP cassette to generate pefrt-Pm-loxP. Finally, pefrt-Pm-loxP was digested with *Asp*718 (Roche Diagnostics, Indianapolis, IN), filled with T4 DNA polymerase, and the blunt-end filled *Cla*I fragment of pMCDTApA (a generous gift from Dr. Yagi, Osaka University, Osaka, Japan) was inserted to the filled *Asp*718 site to create the targeting vector.

Detection of homologous recombination in embryonic stem cells. The targeting vector was digested with *Sac*II for linearization and then transfected into embryonic day 14 embryonic stem (ES) cells with a GenePulser (Bio-Rad, Hercules, CA) at 3 μF and 800 V. Transfected ES cells were plated on neomycin-resistant, mitomycin C-treated mouse embryonic feeder cells (MEFs) in a 10 cm dish. One day after plating, positive selection was performed in the presence of 150 μg/ml geneticin (G418; Invitrogen, Carlsbad, CA). Resistant clones were picked at day 7 and subsequently expanded into 24-well plates preseeded with MEFs. *Bam*HI-digested genomic DNA from individual clones was analyzed by Southern blotting using [α-^{32}P] dCTP-labeled DNA that corresponded to the genomic sequence immediately upstream of the targeting vector as the 5′ probe (Fig. 1*B*). Positive clones were further confirmed by Southern blot analysis using [α-^{32}P] dCTP-labeled DNA that corresponded to the genomic sequence immediately downstream of the targeting vector as the 3′ probe (Fig. 1*B*). The presence of the nonsense mutation was verified by PCR analysis. PCR was performed with 1–100 ng of total genomic DNA, 0.2 mM dNTPs, and 2.5 U of Blend *Taq*-plus polymerase (Toyobo, Osaka, Japan) under the following conditions: 40 cycles of 94°C for 30 s and 60°C for 1 min. The nucleotide sequences of the 5′, RX, and wild-type (WT) primers were 5′-ATGATTCCTAGGGGGATGTC-3′, 5′-TTTACTTTCACATTTTTCCATCA-3′, and 5′-CTTTCACATTTTT-CCACCG-3′, respectively.

Generation of Scn1a knock-in mice. Approximately 10–15 ES cells from one targeted clone (5D8) was injected into C57BL/6J blastocysts. An average of 15 injected blastocysts were transferred into pseudopregnant female recipient ICR mice. The ES clone produced several male chimeras with >50% agouti coat color, which were then bred to C57BL/6 females to allow for the detection of germline transmission. One F1 male heterozygous for the RX mutation was obtained and subsequently crossed with C57BL/6 females to generate N2 *Scn1a*$^{RX/+}$ mice. Homozygous mice (*Scn1a*$^{RX/RX}$) were obtained by interbreeding N2 *Scn1a*$^{RX/+}$ mice.

We used mice resulting from intercrossing N2 *Scn1a*$^{RX/+}$ mice in a C57BL/6/129 (~75%/25%) background in this study, unless stated otherwise.

The neo cassette was removed by injecting pCAGGS-FLPe (Gene Bridges, Heidelberg, Germany) into *in vitro* fertilized eggs, which were derived from an N2 *Scn1a*$^{RX/+}$ male and C57BL/6 females. The absence of the neo cassette was verified by Southern blotting using [α-^{32}P] dCTP-labeled DNA that corresponded to the genomic sequence immediately upstream of exon 23 and the coding sequence of neo cassette as the internal and neo probes, respectively (supplemental Fig. 1*A*, available at www.jneurosci.org as supplemental material).

Electrocorticographic recordings. Electrocorticographic (EcoG) electrodes were implanted using 1.5% halothane anesthesia with N_2O:O_2 (3:2) ventilation. Stainless-steel screws (1.1 mm diameter) served as EcoG electrodes and were secured to the skull and dura over the right somatosensory cortex (1.5 mm lateral to midline, 1.0 mm posterior to bregma) and the cerebellum (at midline, 2.0 mm posterior to lambda) as a reference electrode. EcoG recordings were performed with postnatal day 14 (P14)–P16 *Scn1a*$^{RX/RX}$ and *Scn1a*$^{+/+}$ pups ($n = 3$, each group).

Northern blot analyses. Total RNA was extracted from P14–P16 mouse brains using Trizol reagent (Invitrogen), and poly(A) RNA was affinity purified from total RNA using Fast Track MAG maxi mRNA isolation kit (Invitrogen). Two micrograms of poly(A) RNA were separated by 1.2% agarose formaldehyde gel electrophoresis, and the RNA was transferred to Biodyne nylon membranes (Pall Bio Support, East Hills, NY). The RNA blots were hybridized with three different [α-^{32}P] dCTP-labeled DNA probes [namely, 5′-untranslated region (UTR), coding region, and 3′-UTR probes, respectively] using ULTRAhyb (Ambion, Austin, TX). The 5′-UTR probe was made from PCR product using mouse genomic DNA and 5′-UTR primers, whose nucleotide sequences were 5′-ACATCTCCCCACGACGAGT-3′ and 5′-AGCACTTGGTCACCTTTTGC-3′. The coding region and 3′-UTR probes were made from reverse-transcription PCR products using the total mouse brain cDNA pool as templates. The nucleotide sequences of the coding region primers were 5′-CTCTTCATGGGCAACCTGAG-3′ and 5′-CACATATATCCTTCTGGACATTGG-3′, and those of the 3′-UTR primers were 5′-AGTCTAAAGGGGTGCAGAGC-3′ and 5′-GTCAATTCGCTCTGCTAGGG-3′.

In situ *hybridization.* P14–P16 mice were deeply anesthetized with ether and perfused transcardially with 4% paraformaldehyde-PBS (10 mM phosphate buffer, 2.7 mM KCl, and 137 mM NaCl, pH 7.4). Brains were removed from the skull, postfixed in 4% paraformaldehyde-PBS for 15 h at 4°C, and embedded in paraffin. Sections (6 μm thick) of 4% paraformaldehyde-fixed, paraffin-embedded brains were deparaffinized and incubated with 10 μg/ml proteinase K (Invitrogen) in PBS at room temperature for 15 min. After acetylation, the sections were incubated in hybridization buffer containing 500 ng/ml digoxigenin-labeled riboprobes at 60°C overnight in a humidified chamber. The hybridized sections were washed by successive immersion in 2× SSC, 50% formamide (at 60°C for 20 min, twice), TNE (1 mM EDTA, 500 mM NaCl, 10 mM Tris-HCl, pH 8.0, at 37°C for 10 min), TNE containing 20 μg/ml RNase A (at 37°C for 30 min), 2× SSC (at room temperature for 10 min, twice), and 0.2× SSC (at 60°C for 30 min, twice). The hybridization signals were detected using the digoxigenin detection kit (Roche Diagnostics). The coding region and 3′-UTR riboprobes were made from the reverse transcription-PCR products described in Northern blot analyses using digoxigenin RNA labeling kit (Roche Diagnostics).

Antibody generation. Rabbit polyclonal anti-C-terminal $Na_v1.1$ antibody (IO1) was raised against oligopeptides corresponding to the amino acids IVEKHEQEGKDEKAKGK of mouse $Na_v1.1$ plus C at its N terminus for coupling. Antibody was then affinity purified against oligopeptides HEQEGKDEKAKGK of mouse $Na_v1.1$ plus C at its N terminus using the SulfoLink kit (Pierce, Rockford, IL) to obtain antibody that recognized $Na_v1.1$ specifically (see Results). The antibody was used for Western blot analysis, immunohistochemistry, and immunofluorescence histochemistry. In Western blot analysis and immunohistochemistry, $Na_v1.1$ immunoreactivity was abolished when the antibody was preabsorbed with oligopeptides used for affinity purification (data not shown).

Rabbit polyclonal anti-$Na_v1.6$ antibody was raised against oligopeptides corresponding to the amino acids SEDAIEEEGEDGVGSPRS of rat and mouse $Na_v1.6$ plus C at its N terminus for coupling and then affinity purified using the SulfoLink kit (Pierce) (Caldwell et al., 2000; Krzemien et al., 2000).

Western blot analyses. Brains were isolated from mice at P14–P16 and homogenized in homogenization buffer [0.32 M sucrose, 10 mM HEPES, 2 mM EDTA, and 1× complete protease inhibitor mixture (Roche Diagnostics), pH 7.4]. The homogenates were then centrifuged for 15 min at 1000 × *g*. The supernatants were next centrifuged for 30 min at 30,000 × *g*. The pellets were subsequently resuspended in lysis buffer (50 mM HEPES and 2 mM EDTA, pH 7.4) and centrifuged for 30 min at 30,000 × *g*. Total brain membrane proteins were dissolved in 2 M urea, 1× NuPAGE reducing agent (Invitrogen), and 1× NuPAGE lithium dodecyl sulfate sample buffer (Invitrogen), separated on the NuPAGE Novex Tris-acetate 3–8% gel (Invitrogen) or the polyacrylamide gel mini DAIICHI Tris-glycine 4–20% gel (Daiichi, Tokyo, Japan), transferred to a nitrocellulose membrane (Schleicher & Schull, Dassel, Germany), and immunoblotted. Blots were probed with the rabbit anti-internal-region-$Na_v1.1$ (1:200; Millipore, Billerica, MA), goat anti-internal-region-$Na_v1.1$ (1:100; Santa Cruz Biotechnology, Santa Cruz, CA), rabbit anti-C-terminal $Na_v1.1$ (250 ng/ml), rabbit anti-$Na_v1.2$ (1:100; Alomone, Jerusalem, Israel), goat anti-$Na_v1.3$ (1:100; Santa Cruz Biotechnology), mouse anti-$Na_v1.6$ (1:500; Abnova, Taipei, Taiwan), rabbit anti-pan sodium channel α subunits (1:1000), mouse anti-pan sodium channel α subunits (1:1000; Sigma-Aldrich, St. Louis, MO), rabbit anti-$Na_v2.1$, -$Na_v2.2$, -$Na_v2.3$, and -$Na_v2.4$ (1:1000) (Wong et al., 2005), and mouse anti-β tubulin (1:5000; Sigma-Aldrich) antibodies. The blot was then incubated with horseradish peroxidase-conjugated goat anti-mouse IgG (1:10,000; Promega, Madison, WI), goat anti-rabbit IgG (1:1000; Santa Cruz Biotechnology), or rabbit anti-goat IgG Fc fragment (1:10,000; Jackson ImmunoResearch, West Grove, PA) antibody, and bound antibodies were detected using enhanced chemiluminescence reagent (PerkinElmer, Boston, MA). The rabbit anti-pan sodium channel α subunits, $Na_v2.1$, $Na_v2.2$, $Na_v2.3$ and $Na_v2.4$ antibodies were generous gifts from Drs. Oyama and Nukina (RIKEN Brain Science Institute).

Immunohistochemistry and immunofluorescence histochemistry. Sections (5–6 μm) of 4% paraformaldehyde-fixed, paraffin-embedded P14–P16 mouse brains were deparaffinized, rehydrated, and microwaved in 10 mM citrate acid, pH 6.0, and 1 mM EDTA, pH 8.0, or in 10 mM citrate acid, pH 6.0, 2 mM EDTA, pH 8.0, and 0.05% Tween 20. After incubating the slides with blocking solution (10% goat or donkey serum in PBS) for 1 h at room temperature, sections were incubated with the rabbit anti-internal-region-$Na_v1.1$ (1:1000; Millipore), goat anti-internal-region-$Na_v1.1$ (1:200; Santa Cruz Biotechnology), or rabbit anti-C-terminal $Na_v1.1$ (250 ng/ml) antibody in a humidified chamber for 12 h at 4°C. Endogenous peroxidases were quenched by incubation with 0.3% hydrogen peroxide in PBS. The sections were then incubated with biotinylated goat or donkey polyclonal secondary antibody (1:200; Vector Laboratories, Burlingame, CA). Detection of antibody–antigen complexes was accomplished using the Vectastain Elite ABC kit (Vector Laboratories) and the metal-enhanced DAB substrate kit (Pierce).

Immunofluorescence histochemistry was performed as described above, except that the primary antibody was the rabbit anti-C-terminal $Na_v1.1$ antibody (250 ng/ml) and that the secondary antibodies were Alexa Flour 488, 594, and 647 conjugated (1:400; Invitrogen). Parvalbumin, βIV-spectrin, phosphorylated neurofilament, $Na_v1.6$, and Kv1.2 were detected with the mouse anti-parvalbumin antibody (1:2000; Swant, Bellinzona, Switzerland), chicken anti-βIV spectrin antibody (1:100) (Komada and Soriano, 2002), mouse anti-phosphorylated neurofilament antibody mixture (SMI312) (1:1000; Covance, Berkeley, CA), rabbit anti-$Na_v1.6$ antibody (10 μg/ml) (Caldwell et al., 2000; Krzemien et al., 2000), and mouse anti-Kv1.2 antibody (1:1000; NeuroMab, Davis, CA), respectively. Images were taken with a TCS SP2 microscope (Leica Microsystems, Wetzlar, Germany) and processed with Adobe Photoshop Elements 3.0 (Adobe Systems, San Jose, CA). The chicken anti-βIV spectrin antibody was a generous gift from Dr. Komada (Tokyo Institute of Technology, Tokyo, Japan).

Current-clamp analysis. Coronal slices (350 μm) of binocular visual cortex were cut under halothane anesthesia from both *Gad1*$^{GFP/+}$:

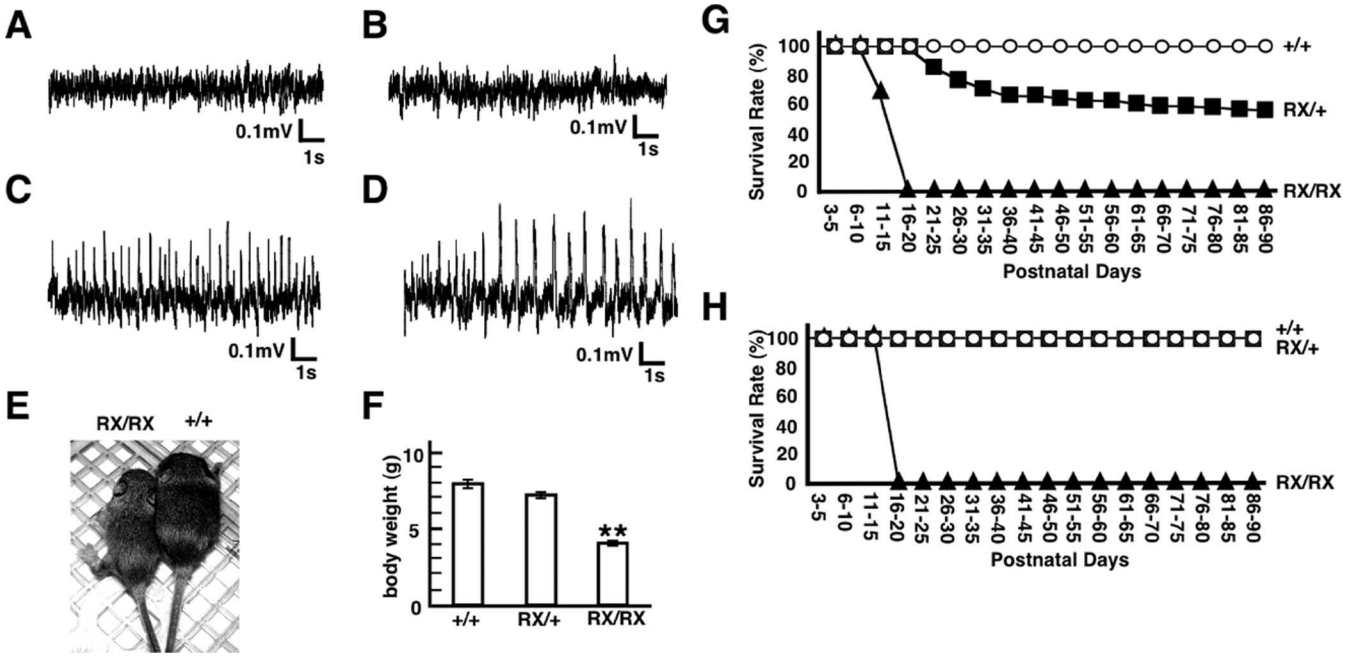

Figure 2. *Scn1a*$^{RX/RX}$ mice developed spontaneous seizures, were malnourished, and died prematurely. ***A***, Representative EcoG recorded in a P14.5 *Scn1a*$^{+/+}$ pup. ***B***, Representative interictal EcoG recorded in a P14.5 *Scn1a*$^{RX/RX}$ pup. ***C***, ***D***, Two examples of ictal EcoG recorded in two P14.5 *Scn1a*$^{RX/RX}$ pups. ***E***, Photographs of an *Scn1a*$^{RX/RX}$ pup (left) and its wild-type littermate (right) at P14.5. ***F***, Body weight of *Scn1a*$^{+/+}$ ($n = 15$), *Scn1a*$^{RX/+}$ ($n = 40$), and *Scn1a*$^{RX/RX}$ ($n = 23$) pups at P14.5. Body weight was significantly reduced in *Scn1a*$^{RX/RX}$ pups compared with their *Scn1a*$^{+/+}$ and *Scn1a*$^{RX/+}$ littermates (**$p < 0.01$). Values represent means ± SEM. ***G***, Survival curves of *Scn1a*$^{+/+}$ (open circles; $n = 26$), *Scn1a*$^{RX/+}$ (filled rectangles; $n = 50$), and *Scn1a*$^{RX/RX}$ (filled triangles; $n = 19$) mice in a C57BL/6/129 (75%/25%) background from P3. ***H***, Survival curves of *Scn1a*$^{+/+}$ (open circles; $n = 8$), *Scn1a*$^{RX/+}$ (filled rectangles; $n = 23$), and *Scn1a*$^{RX/RX}$ (filled triangles; $n = 8$) mice in a C57BL/6/129 (25%/75%) background from P3.

Scn1a$^{+/+}$ (WT) and *Gad1*$^{GFP/+}$:*Scn1a*$^{RX/+}$ (HET) mice at P25–P29. Slices were incubated in oxygenated (95% O_2, 5% CO_2) artificial CSF (>1 h, 22–25°C) containing the following (in mM): 119 NaCl, 2.5 KCl, 1.3 $MgSO_4$, 1.0 NaH_2PO_4, 26.2 $NaHCO_3$, 2.5 $CaCl_2$, and 11 glucose. Then, they were placed in a submersion chamber for recording at room temperature (~25°C). Once a fluorescent interneuron from layer II/III was selected using fluorescent microscopy, it was visualized with infrared-differential interference contrast optics (BX50WI; Olympus, Hamamatsu, Japan) and recorded with conventional current-clamp techniques. The electrodes (tip resistance of 7–10 MΩ) were filled with solution containing the following (in mM): 126 K-gluconate, 0.2 EGTA, 20 HEPES, 0.5 Na_3GTP, 3 MgATP, 2 NaCl, 8 KCl, and 0.15% biocytin. The pH was adjusted to 7.2–7.4 with KOH. Recordings were filtered at 1 kHz, digitized at 10 kHz, stored, and analyzed using Experimenter's Workbench (DataWave Technologies, Longmont, CO). Data are given as mean ± SEM. Differences were considered statistically significant using Student's *t* test if $p < 0.05$.

Electrophysiological properties of neurons were identified in response to injection of positive or negative square current pulses lasting 500 ms. Each current pulse injection was repeated five times with 10 s intervals. First, small positive currents were applied to find out a threshold to trigger an action potential. Then, bigger positive currents were applied to look at frequency adaptation of cells. Negative current pulses were applied between positive current pulses. Electrophysiological data were assigned to cell type on the basis of whole-cell biocytin fills during each recording. Slices that contained stained cells were fixed overnight in 4% paraformaldehyde at 4°C and reacted with streptavidin and Alexa Flour 546 conjugate (Invitrogen). Spike decrement was calculated as percentage of last spike amplitude divided by first spike amplitude. Eight neurons (taken from eight animals) were recorded for both WT and HET mice.

Results

Unstable gait, spontaneous seizures, and premature death in *Scn1a* knock-in mice

A knock-in mouse line carrying a premature stop codon, R1407X, in exon 21 of the *Scn1a* gene was generated and characterized (Fig. 1). We choose the RX mutation because this mutation is identical to a pathogenic mutation found in three unrelated SMEI patients (Sugawara et al., 2002; Fujiwara et al., 2003; Fukuma et al., 2004) and the mutant $Na_v1.1$ expressed heterologously in HEK293 cells was inactive in channel function (Sugawara et al., 2003). The RX mutation, therefore, should be representative of SMEI mutations.

Homozygous knock-in (*Scn1a*$^{RX/RX}$) pups were born in approximated expected Mendelian ratios (supplemental Table 1, available at www.jneurosci.org as supplemental material). *Scn1a*$^{RX/RX}$ pups were viable and physically indistinguishable from their *Scn1a*$^{+/+}$ and *Scn1a*$^{RX/+}$ littermates in the first postnatal week. However, *Scn1a*$^{RX/RX}$ pups subsequently developed recurrent spontaneous seizures at P12, whereas no epileptic seizure phenotypes were seen in their age-matched *Scn1a*$^{+/+}$ and *Scn1a*$^{RX/+}$ littermates. *Scn1a*$^{RX/RX}$ pups showed tonic-clonic and clonic seizures at P12–P16; they suffered rhythmic jerking movements and involuntary muscle contraction. Typically, the seizure duration was 1–3 min, and the intervals between seizure attacks were ~1–4 h. To confirm that these episodes were, in fact, seizures, we performed EcoG recordings of freely moving mice using P14–P16 *Scn1a*$^{RX/RX}$ and *Scn1a*$^{+/+}$ pups. EcoG analysis of *Scn1a*$^{RX/RX}$ pups demonstrated not only background activities similar to those of *Scn1a*$^{+/+}$ pups (Fig. 2*A*,*B*), but also ictal EcoG patterns consisting of 1–4 Hz polyspike-wave discharges (Fig. 2*C*,*D*). The appearances of abnormal EcoG patterns coincided with those of rhythmic jerking movements.

Furthermore, at p10, *Scn1a*$^{RX/RX}$ pups developed abnormal and unstable gait that apparently brought to *Scn1a*$^{RX/RX}$ pups the disadvantage in competition for feeding with their *Scn1a*$^{+/+}$ and *Scn1a*$^{RX/+}$ littermates. *Scn1a*$^{RX/RX}$ pups became progressively malnourished from P10 and showed, at P14–P15, an ~40% reduction in body weight compared with their *Scn1a*$^{+/+}$ and

Scn1a$^{RX/+}$ littermates (Fig. 2*E*,*F*). The *Scn1a*$^{RX/RX}$ gastrointestinal content was markedly smaller than their *Scn1a*$^{+/+}$ and *Scn1a*$^{RX/+}$ littermates. Eventually, all *Scn1a*$^{RX/RX}$ pups died within the third postnatal week, and we calculated a mean lifetime of 15.8 ± 0.8 d (n = 19) for these mice (Fig. 2*G*). Some *Scn1a*$^{RX/RX}$ pups in the smaller litters were moderately malnourished but still died prematurely.

Although *Scn1a*$^{RX/+}$ pups did not generally suffer seizures until the beginning of the third postnatal week, some individuals exhibited recurrent spontaneous seizures after P18. After P18, sporadic sudden death was also observed in many *Scn1a*$^{RX/+}$ mice, and ~25% and 40% died within the first and third postnatal months, respectively (Fig. 2*G*).

Because mouse strain differences in seizure susceptibility have been described (Schauwecker, 2002), we examined genetic background effects on the abnormal phenotypes. We backcrossed an F1 *Scn1a*$^{RX/+}$ male in a C57BL/6/129 (50%/50%) background to 100% of 129 females to generate N2 *Scn1a*$^{RX/+}$ mice in a C57BL/6/129 (~25%/75%) background. The N2 *Scn1a*$^{RX/+}$ mice do not show premature lethal phenotype, indicating that genetic backgrounds might have modest effects on seizure susceptibility in the case of heterozygous mice. We also generated *Scn1a*$^{RX/RX}$ mice in a C57BL/6/129 (~25%/75%) background by intercrossing N2 *Scn1a*$^{RX/+}$ mice and observed that, like the *Scn1a*$^{RX/RX}$ pups in a C57BL/6/129 (~75%/25%) background, these mice also showed unstable gait, spontaneous seizures, and malnutrition. All mice suffered premature death within the third postnatal week (Fig. 2*H*), and we calculated a mean lifetime of 17.0 ± 0.8 d (n = 8) for these mice. These results suggest that in the case of homozygous mice, there might be minimal genetic background effects on phenotype.

To rule out the possibility that the presence of the neo cassette in the mouse genome might, by some unknown mechanisms, contribute to spontaneous epileptic seizures and premature death of *Scn1a* knock-in mice, the frt-flanked neo cassette was removed from the genome of *Scn1a* knock-in mice (supplemental Fig. 1, available at www.jneurosci.org as supplemental material). Four F1 *Scn1a*$^{RX/+}$ mice in a C57BL/6/129 background (~87.5%/12.5%) lacking the neo cassette were obtained. Two of these died within the third month after birth. A neo-lacking F1 *Scn1a*$^{RX/+}$ female was then crossed with a C57BL/6 male. Analysis of the viability of neo-lacking N2 *Scn1a*$^{RX/+}$ mice showed that some developed spontaneous epileptic seizures and suffered premature deaths, suggesting that the phenotypes of the neo-lacking *Scn1a* knock-in mice do not differ significantly from those of the neo-containing *Scn1a* knock-in mice.

Loss of $Na_v1.1$ protein expression in homozygous knock-in mice

We performed Northern blot analyses of brain mRNA using three different probes, which were targeted against the 5′ untranslated, coding, and 3′ untranslated regions of mouse *Scn1a* mRNA, respectively. As shown in Figure 3*A*, *Scn1a* mRNA expression in *Scn1a*$^{RX/RX}$ pups was significantly lower than that in *Scn1a*$^{+/+}$ pups. *Scn1a* mRNA was apparently expressed at low levels in *Scn1a*$^{RX/RX}$ pups, because *Scn1a* mRNA expression was detected in *Scn1a*$^{RX/RX}$ pups by reverse transcriptase-PCR analysis, and the existence of the RX mutation was confirmed by sequencing the amplicons (our unpublished results). We then analyzed brain membrane proteins by Western blot analyses using three different anti-$Na_v1.1$ antibodies. Two were raised against internal region and one was raised against C terminus. As shown in Figure 3, *B* and *C*, and supplemental Figure 2 (available at www.jneurosci.org as supplemental material), whereas full-length $Na_v1.1$ expression level was high, moderate, and negligible in *Scn1a*$^{+/+}$, *Scn1a*$^{RX/+}$, and *Scn1a*$^{RX/RX}$ pups, respectively, truncated mutant $Na_v1.1$ expression was under a detectable level in *Scn1a*$^{RX/+}$ and *Scn1a*$^{RX/RX}$ pups. These results suggest that the mutant *Scn1a* allele is effectively inactivated in the knock-in mice.

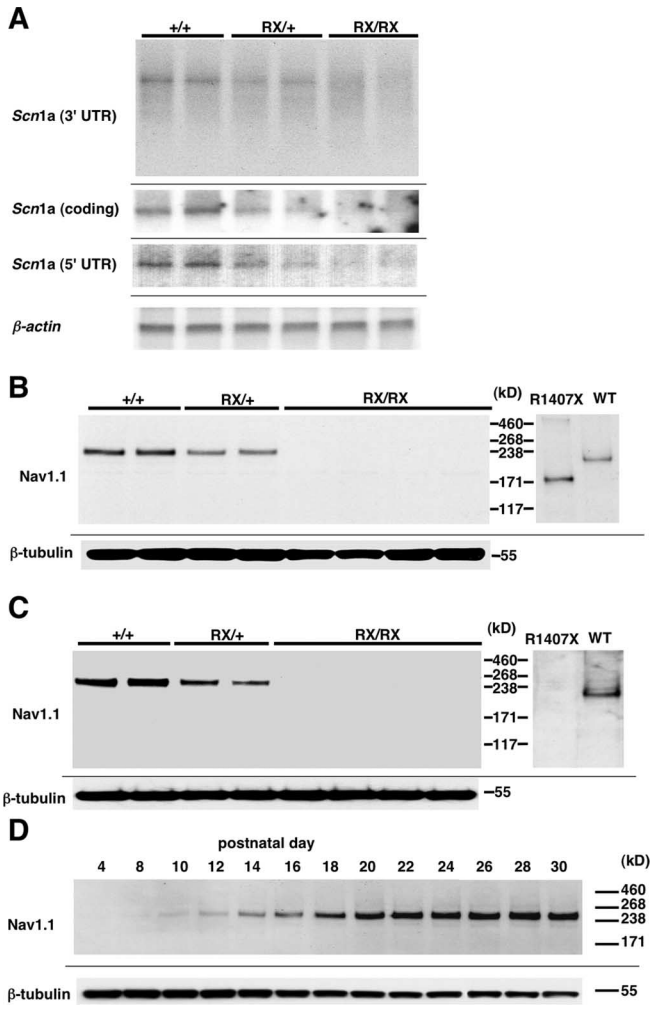

Figure 3. Expression of *Scn1a* mRNA and $Na_v1.1$ protein in P14–P16 *Scn1a*$^{+/+}$, *Scn1a*$^{RX/+}$, and *Scn1a*$^{RX/RX}$ pups. ***A***, Northern blot analyses of total brain poly(A) RNA were performed with three different probes (namely, 5′-UTR, coding region, and 3′-UTR probes, respectively). *β-Actin* was used as internal control. ***B***, Western blot analysis of total brain membrane fraction using the goat anti-internal region $Na_v1.1$ polyclonal antibody (left). This antibody recognized both full-length and truncated mutant $Na_v1.1$ expressed heterologously in HEK293 cells (right). Note that the rabbit anti-internal region $Na_v1.1$ antibody provided an identical pattern (supplemental Fig. 2, available at www.jneurosci.org as supplemental material). β-Tubulin was used as internal control. ***C***, Western blot analysis of total brain membrane fraction using the rabbit anti-C-terminal $Na_v1.1$ polyclonal antibody (left). This antibody recognized full-length $Na_v1.1$ but not truncated mutant $Na_v1.1$ expressed heterologously in HEK293 cells (right). β-Tubulin was used as internal control. ***D***, The developmental expression of $Na_v1.1$ protein in the wild-type mouse brain at different stages. Western blot analysis of total brain membrane fraction was performed with the rabbit anti-C-terminal $Na_v1.1$ polyclonal antibody. β-Tubulin was used as internal control.

The observation that *Scn1a*$^{RX/RX}$ and *Scn1a*$^{RX/+}$ mice appeared to be worsened progressively in the first postnatal month led us to investigate change in the $Na_v1.1$ expression level in wild-type pups during early development with Western blot analysis. Figure 3*D* showed that $Na_v1.1$ expression level was very low at P4, steeply increased during the second and third postnatal weeks, and reached peak before P30. Notably, the onset of unsta-

ble gait and spontaneous seizures coincided with that of dramatic $Na_v1.1$ upregulation.

Western blot analyses also showed no significant changes in $Na_v1.2$, $Na_v1.3$, $Na_v1.6$, total sodium channel α subunit, $Na_v2.1$, $Na_v2.2$, $Na_v2.3$ and $Na_v2.4$ expression levels in *Scn1a*$^{RX/RX}$ pups compared with *Scn1a*$^{+/+}$ littermates (supplemental Fig. 3, available at www.jneurosci.org as supplemental material), suggesting that the absence of $Na_v1.1$ did not markedly alter the basal expression levels of other sodium channel subunits. The total sodium channel α subunit expression was not significantly reduced probably because $Na_v1.1$ accounted for only 10% of total brain sodium channel α subunits (Gordon et al., 1987), and our analyses might lack the sensitivity to detect 10% expression level differences.

Cresyl violet stainings of paraformaldehyde-fixed brain slices from *Scn1a*$^{RX/RX}$ pups (supplemental Fig. 4*A*, available at www.jneurosci.org as supplemental material) showed neither gross anatomical abnormalities nor marked alterations in neuronal cell density compared with their wild-type and heterozygous littermates. However, *Scn1a*$^{RX/RX}$ pups tended to have slightly smaller brains than age-matched *Scn1a*$^{+/+}$ and *Scn1a*$^{RX/+}$ littermates, probably because of a secondary effect of malnutrition (supplemental Fig. 4*B*, available at www.jneurosci.org as supplemental material).

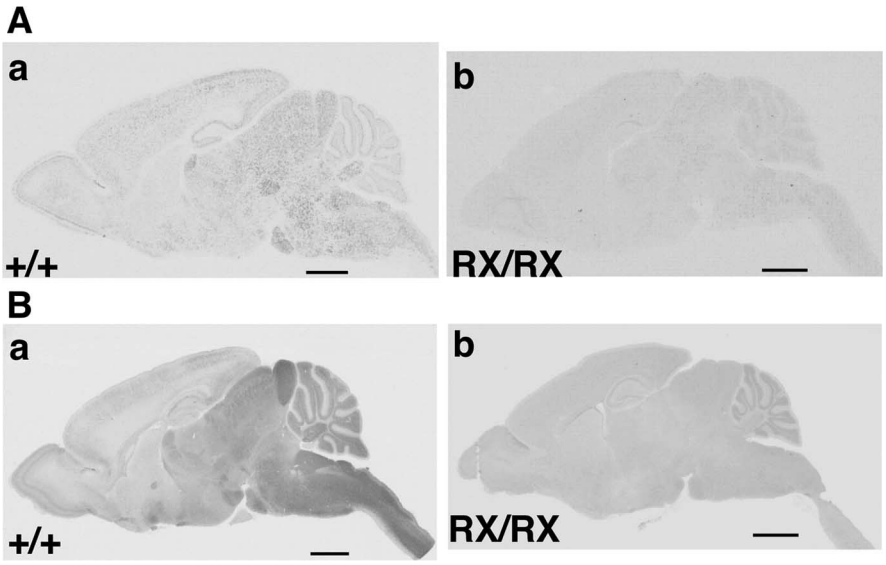

Figure 4. Regional distribution of *Scn1a* mRNA and $Na_v1.1$ protein in the developing mouse brain. ***A***, Detection of *Scn1a* mRNA expression in P14–P16 *Scn1a*$^{+/+}$ (***a***) and *Scn1a*$^{RX/RX}$ pups (***b***) by *in situ* hybridization with the probe complementary to 3′-UTR of *Scn1a* mRNA. Note that *in situ* hybridization with another probe complementary to *Scn1a* mRNA coding region gave an identical pattern (supplemental Fig. 5, available at www.jneurosci.org as supplemental material). Higher-magnified images are also shown in supplemental Figure 6 (available at www.jneurosci.org as supplemental material). Scale bars, 1 mm. ***B***, Detection of $Na_v1.1$ protein in P14–P16 *Scn1a*$^{+/+}$ (***a***) and *Scn1a*$^{RX/RX}$ (***b***) pups by immunohistochemistry with the rabbit anti-C-terminal $Na_v1.1$ antibody. Note that the anti-internal region $Na_v1.1$ antibodies provided an identical staining (supplemental Fig. 7*A*,*B*, available at www.jneurosci.org as supplemental material). Higher-magnified images are also shown in Figures 5*A*, 6*A*, and 7*A* and supplemental Figure 8*A* (available at www.jneurosci.org as supplemental material). Scale bars, 1 mm.

Heterogeneous regional distribution of *Scn1a* mRNA and $Na_v1.1$ protein in the developing mouse brains

We performed *in situ* hybridization using two different probes complementary to the 3′-UTR and coding sequence of mouse *Scn1a* mRNA. Both probes showed intermediate hybridization signal levels to brain sections in an identical distribution pattern. *Scn1a* mRNA expression was relatively high in thalamus, superior colliculus, inferior colliculus, deep cerebellar nuclei, pons, medulla, and spinal cord, whereas it was low in hippocampus, cerebral cortex, and cerebellum (Fig. 4*Aa*; supplemental Figs. 5*A*, 6, available at www.jneurosci.org as supplemental material). These observations were consistent with the results of previous *in situ* hybridization [Beckh et al., 1989; Furuyama et al., 1993; Black et al., 1994; the Allen brain atlas (www.brain-map.org)]. In addition, homozygous knock-in mice showed no obvious *in situ* hybridization signals (supplemental Figs. 4*Ab*, 5*b*, available at www.jneurosci.org as supplemental material), indicating the high specificity of cellular *Scn1a* mRNA localization in the present study.

We next examined $Na_v1.1$ distribution in the developing (P14–P16) mouse brains by means of immunohistochemistry using three different anti-$Na_v1.1$ antibodies (Fig. 4*Ba*; supplemental Fig. 7*Aa*,*Ba*, available at www.jneurosci.org as supplemental material). The three antibodies gave an identical staining pattern with low-to-moderate signal intensity over the brain regions. The $Na_v1.1$ immunostaining was relatively intense in the caudal brain parts, including thalamus, superior colliculus, inferior colliculus, pons, medulla, deep cerebellar nuclei, and spinal cord. This $Na_v1.1$ protein distribution in the brain agreed with the *Scn1a* mRNA distribution as described above (Fig. 4*Aa*). Although a previous study showed the homogenous brain distribution of $Na_v1.1$ (Westenbroek et al., 1989) (see Discussion), we verified the specificity of our immunohistochemistry by using the $Na_v1.1$-deficient homozygous knock-in mice as negative controls (Fig. 4*Bb*; supplemental Fig. 7*Ab*,*Bb*, available at www.jneurosci.org as supplemental material).

$Na_v1.1$ protein clusters predominantly at axon initial segments of parvalbumin-positive interneurons in the developing mouse neocortex

In neocortex, the intense $Na_v1.1$-immunoreactive fibers were observed, and some apparently originated from somata of some neurons (Fig. 5*Aa*,*Ab*; supplemental Fig. 7*C*,*D*). Because only a subpopulation of neocortical neurons seemed to have the $Na_v1.1$-immunoreactive signals in the proximal portion of their neurites, we assumed that these neurons belong to some of the interneuron subtypes. Examination of $Na_v1.1$ localization with interneuron markers, including somatostatin, calretinin, and parvalbumin, revealed that the $Na_v1.1$-immunoreactive fibers were PV interneuron specific (Fig. 5*Ba*,*Bc*,*Bd* and our unpublished results).

We assumed that the immunoreactive signals for $Na_v1.1$ were concentrated at axon initial segments (AISs) of the nerve fiber, as judged from their pronounced localization in the proximal portion of the neurites. Examination of $Na_v1.1$ colocalization with βIV-spectrin, which is associated with ankyrin-G and specifically clustered at AISs and nodes of Ranvier (Berghs et al., 2000; Komada and Soriano, 2002; Inda et al., 2006), revealed that the $Na_v1.1$-immunoreactive portions of the nerve fibers were the βIV-spectrin-immunoreactive AISs of PV interneurons (Fig. 5*Ba*,*Bb*,*Bd*). Notably, $Na_v1.1$ immunoreactivities were undetec-

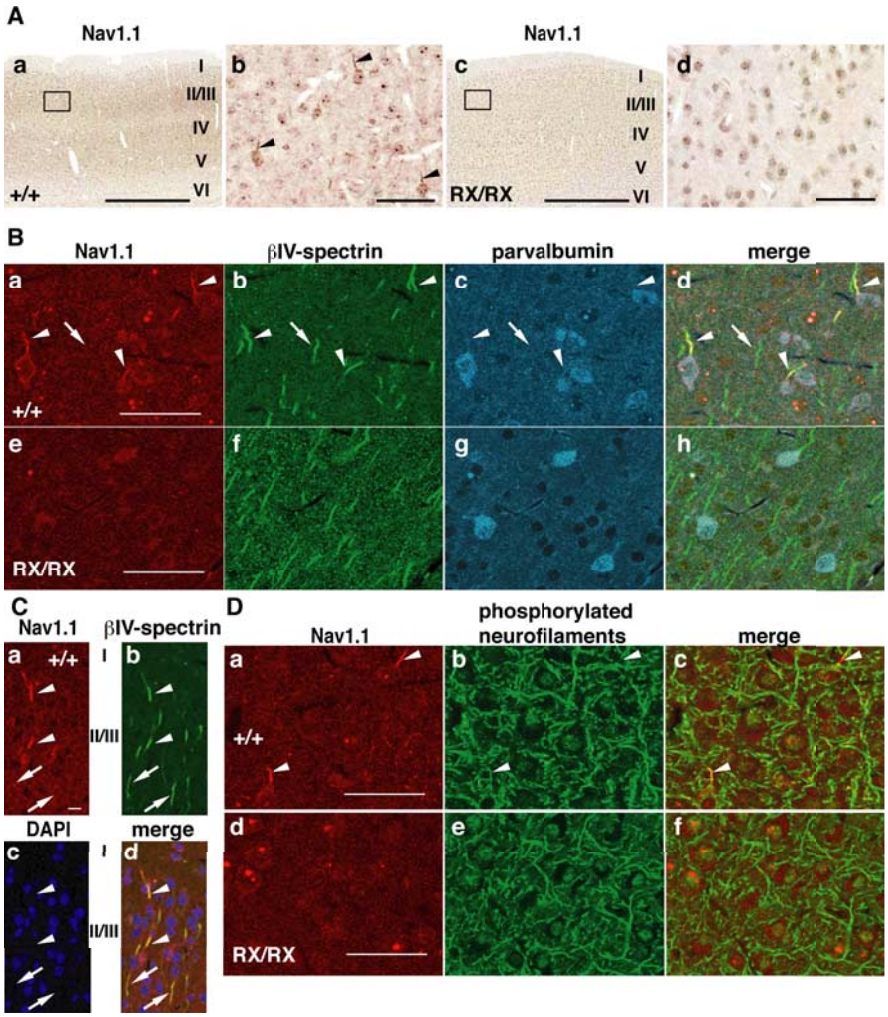

Figure 5. $Na_v1.1$ localization to AISs of parvalbumin-positive interneurons in the developing neocortex. P14–P16 *Scn1a*$^{+/+}$ and *Scn1a*$^{RX/RX}$ pups were examined. Shown are representative images. Arrowheads indicate examples of $Na_v1.1$-immunoreactive AISs. ***A***, Neocortices of *Scn1a*$^{+/+}$ (***a***) and *Scn1a*$^{RX/RX}$ (***c***) pups were stained using the rabbit anti-C-terminal $Na_v1.1$ antibody and DAB. ***b***, ***d***, Higher-magnified images outlined in ***a*** and ***c***. Scale bars: ***a***, ***c***, 500 μm; ***b***, ***d***, 40 μm. ***B***, Immunofluorescence histochemistry with the rabbit anti-C-terminal $Na_v1.1$ antibody (***a***, ***e***; red), together with the anti-βIV-spectrin (***b***, ***f***; green) and anti-parvalbumin (***c***, ***g***; blue) antibodies. ***d***, ***h***, Merged images. ***a–d***, Arrows indicate examples of AISs immunopositive for βIV-spectrin but not for $Na_v1.1$. Scale bars, 50 μm. ***C***, Immunofluorescence histochemistry with the rabbit anti-C-terminal $Na_v1.1$ (***a***; red) and anti-βIV-spectrin (***b***; green) antibodies, together with 4′-6-diamidino-2-phenylindole (DAPI) (***c***; blue). ***d***, Merged images. Arrows indicate examples of AISs immunopositive for βIV-spectrin but not for $Na_v1.1$. Scale bars, 10 μm. ***D***, Immunofluorescence histochemistry with the rabbit anti-C-terminal $Na_v1.1$ antibody (***a***, ***d***; red), together with the anti-phosphorylated neurofilament antibody mixture (SMI312) (***b***, ***e***; green). ***c***, ***f***, Merged images. Scale bars, 50 μm. All images are oriented from pial surface (top) to callosal (bottom).

ted in almost all of the βIV-spectrin-immunoreactive fibers that seemed to be pyramidal cell AISs (Fig. 5*C*) (Komada and Soriano, 2002).

To further confirm $Na_v1.1$ localization to AISs, we examined $Na_v1.1$ colocalization with phosphorylated neurofilaments, which are distributed to selected axons (Sternberger and Sternberger, 1983; Ulfig et al., 1998). Expectedly, $Na_v1.1$-immunoreactive AISs were also phosphorylated neurofilament immunoreactive (Fig. 5*Da–Dc*). Together, these results indicate that $Na_v1.1$ in the developing neocortex is predominantly localized at AISs of PV interneurons.

Some $Na_v1.1$-immunoreactive fibers scattered in the layer II/III did not colocalize with βIV-spectrin and, therefore, they seemed not to be AISs. Although these fibers remained uncharacterized, these fibers might be distal axons because of a generality of $Na_v1.1$ localization to axons in the developing mouse brains (see below).

$Na_v1.1$ protein localizes largely to somata and axons of parvalbumin-positive interneurons in the developing mouse hippocampus

In hippocampus, somata of nonpyramidal cells and fibers scattered in stratum oriens, pyramidale, and radiatum were $Na_v1.1$ immunoreactive moderately, whereas $Na_v1.1$ immunoreactivities of pyramidal cell somata were negligible (Fig. 6*Aa*,*Ab*). These observations are consistent with the results of *in situ* hybridization (see supplemental Fig. 6, available at www.jneurosci.org as supplemental material) but different from those of previous immunohistochemistry, suggesting that $Na_v1.1$ is expressed in both pyramidal and nonpyramidal cells (Westenbroek et al., 1989; Gong et al., 1999; Yu et al., 2006) (see Discussion).

Examination of $Na_v1.1$ colocalization with parvalbumin revealed that nearly all (54 of 55; 98.2%) PV interneurons had $Na_v1.1$-immunoreactive somata and that PV interneurons composed the majority (54 of 71; 76.1%) of $Na_v1.1$-immunoreactive cells (Fig. 6*Ba*,*Bc*,*Bd*). Some relatively long $Na_v1.1$-immunoreactive fibers scattered in stratum oriens and pyramidale were parvalbumin immunoreactive weakly but not βIV-spectrin immunoreactive (Fig. 6*Be–Bh*). These fibers were phosphorylated neurofilament immunoreactive (Fig. 6*Ca–Cc*), suggesting possible $Na_v1.1$ localization to distal axons of PV interneurons. In other cases, $Na_v1.1$-immunoreactive fibers were βIV-spectrin immunoreactive and located at the AISs of PV interneurons (Fig. 6*Bi–Bl*). These results indicate that $Na_v1.1$ in hippocampus is largely localized to somata and, perhaps, proximal and distal axons of nonpyramidal cells, the majority of which are PV interneurons.

Subcellular localization of $Na_v1.1$ protein in the developing mouse cerebellum

In cerebellum, we observed strongly $Na_v1.1$-immunoreactive fibers, which were also immunoreactive for both βIV-spectrin and phosphorylated neurofilaments (Fig. 7*A*,*Ba–Bd*,*C*). These were distributed in inner portion of the molecular layer, close to the Purkinje cell somata. Normally, intense $Na_v1.1$ immunoreactivity was located in a part of the fiber in which the immunoreactivity for βIV-spectrin was weak or undetectable. Therefore, $Na_v1.1$ seems to be largely localized to distal axons. Because the $Na_v1.1$-immunoreactive fibers were located in the lower molecular layer, they appear to be axons of basket cells (Bishop, 1993).

Moreover, the $Na_v1.1$-immunoreactive signals were visible on the proximal portion of βIV-spectrin-immunoreactive AISs of Purkinje cells (Fig. 7*Be–Bh*). These observations are consistent with the results of a previous study showing the reduction in

whole-cell sodium current densities in dissociated Purkinje cells of $Na_v1.1$-null mice (Kalume et al., 2005).

We also observed strongly $Na_v1.1$-immunoreactive puncta, which were immunoreactive for βIV-spectrin as well, in cerebellar fastigial, interpositus, and lateral deep nuclei and white matter (supplemental Fig. 8*A*,*B*, available at www.jneurosci.org as supplemental material). Examination of $Na_v1.1$ localization with Kv1.2, which is normally restricted to the juxtaparanodes flanking nodal βIV-spectrin in cerebellar white matter (Lacas-Gervais et al., 2004), revealed that the $Na_v1.1$-immunoreactive puncta localized to a subpopulation of nodes of Ranvier in cerebellar white matter (supplemental Fig. 8*Da–Dd*, available at www.jneurosci.org as supplemental material). Moreover, the $Na_v1.1$ immunoreactivities were undetectable in the βIV-spectrin-immunoreactive AISs of Kv1.2-immunoreactive neurons of deep cerebellar nuclei (supplemental Fig. 8*De–Dh*, available at www.jneurosci.org as supplemental material). These observations further support $Na_v1.1$ localization at the nodes of Ranvier in the cerebellar white matter and deep nuclei.

Furthermore, in developing corpus callosum and fimbria, we observed $Na_v1.1$-immunoreactive puncta, which were immunoreactive for βIV-spectrin as well (our unpublished results). These observations suggest that $Na_v1.1$ might be predominantly localized at the nodes of Ranvier in corpus callosum and fimbria.

Altogether, these results show a generality of $Na_v1.1$ localization to axons in the developing mouse brains but distinct from the results of previous immunohistochemical analyses indicating somatodendritic $Na_v1.1$ localization (Westenbroek et al., 1989; Gong et al., 1999) (see Discussion).

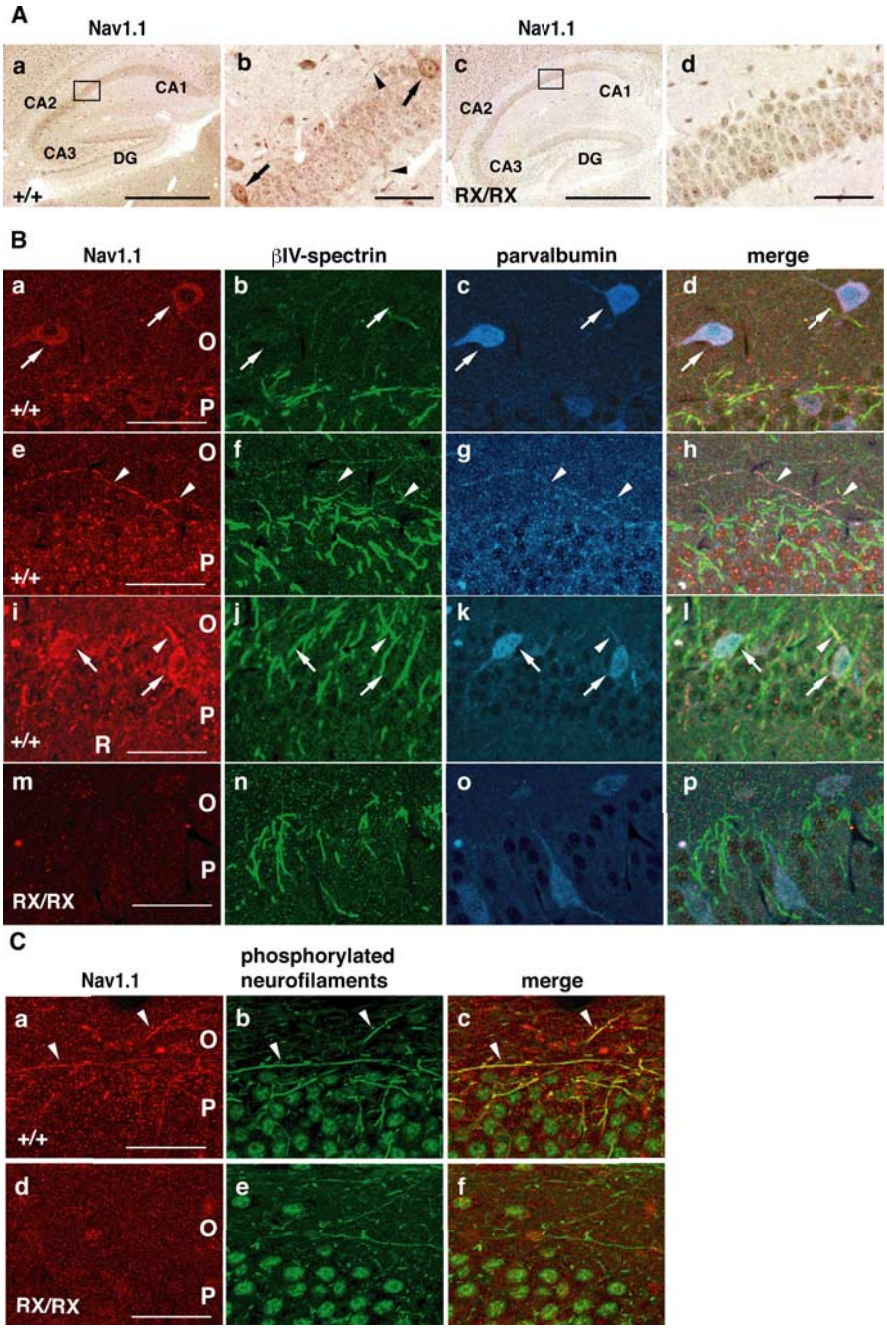

Figure 6. $Na_v1.1$ localization to somata and axons of parvalbumin-positive interneurons in the developing hippocampus. P14–P16 *Scn1a*$^{+/+}$ and *Scn1a*$^{RX/RX}$ pups were examined. Shown are representative images. Arrowheads and arrows indicate examples of $Na_v1.1$-immunoreactive fibers and somata, respectively. ***A***, Hippocampi of *Scn1a*$^{+/+}$ (***a***) and *Scn1a*$^{RX/RX}$ (***c***) pups were stained using the rabbit anti-C-terminal $Na_v1.1$ antibody and DAB. ***b***, ***d***, Higher-magnified images outlined in ***a*** and ***c***. Scale bars: ***a***, ***c***, 500 μm; ***b***, ***d***, 40 μm. ***B***, Immunofluorescence histochemistry with the rabbit anti-C-terminal $Na_v1.1$ antibody (***a***, ***e***, ***i***, ***m***; red), together with the anti-βIV-spectrin (***b***, ***f***, ***j***, ***n***; green) and anti-parvalbumin (***c***, ***g***, ***k***, ***o***; blue) antibodies. ***d***, ***h***, ***l***, ***p***, Merged images. Scale bars, 50 μm. ***C***, Immunofluorescence histochemistry with the rabbit anti-C-terminal $Na_v1.1$ antibody (***a***, ***d***; red), together with the anti-phosphorylated neurofilament antibody mixture (SMI312) (***b***, ***e***; green). ***c***, ***f***, Merged images. Scale bars, 50 μm. DG, Dentate gyrus; O, stratum oriens; P, stratum pyramidale; R, stratum radiatum.

Rapid amplitude decrement in the spike trains in heterozygous neocortical fast-spiking interneurons

We examined whether reduced $Na_v1.1$ expression altered the firing properties of neocortical PV interneurons, which would also be regarded as fast-spiking interneurons (Kawaguchi and Kondo, 2002), using patch-clamp recordings from neurons in mouse neocortical slices. To facilitate identification of PV, fast-spiking interneurons, we crossed N2 *Scn1a*$^{+/RX}$ mice with heterozygous GAD67-GFP (Δneo) mice (*Gad1*$^{GFP/+}$ mice) (Tamamaki et al., 2003) in a C57BL/6/129 (~75%/25%) background to obtain *Gad1*$^{GFP/+}$:*Scn1a*$^{+/+}$ and *Gad1*$^{GFP/+}$:*Scn1a*$^{RX/+}$ mice. The phenotypes of the *Gad1*$^{GFP/+}$:*Scn1a*$^{RX/+}$ mice do not differ significantly from those of the *Gad1*$^{+/+}$:*Scn1a*$^{RX/+}$ mice.

No difference in input resistance, average spike half-width, or threshold was observed between *Gad1*$^{GFP/+}$:*Scn1a*$^{+/+}$ and *Gad1*$^{GFP/+}$:*Scn1a*$^{RX/+}$ interneurons ($n = 8$, each group). Single-spike amplitude was also similar in the two groups. However, during prolonged spike trains, spike amplitude decrement was pronounced in *Gad1*$^{GFP/+}$:*Scn1a*$^{RX/+}$ interneurons (Fig. 8*A*,*B*).

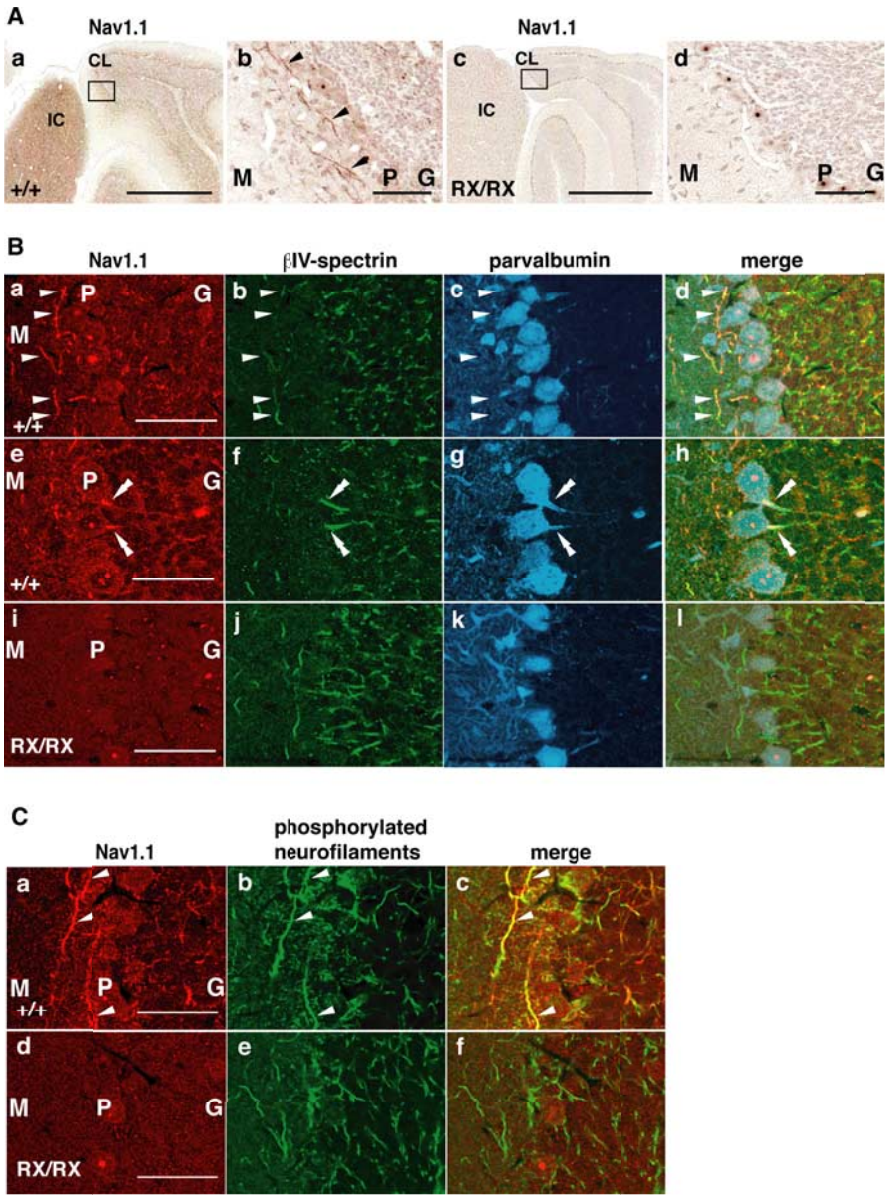

Figure 7. $Na_v1.1$ localization to axons in the developing cerebellar cortex. P14–P16 *Scn1a*$^{+/+}$ and *Scn1a*$^{RX/RX}$ pups were examined. Shown are representative images. Arrowheads indicate examples of $Na_v1.1$-immunoreactive fibers. ***A***, Cerebellar cortices of *Scn1a*$^{+/+}$ (***a***) and *Scn1a*$^{RX/RX}$ (***c***) pups were stained using the rabbit anti-C-terminal $Na_v1.1$ antibody and DAB. ***b***, ***d***, Higher-magnified images outlined in ***a*** and ***c***. Scale bars: ***a***, ***c***, 500 μm; ***b***, ***d***, 40 μm. ***B***, Immunofluorescence histochemistry with the rabbit anti-C-terminal $Na_v1.1$ antibody (***a***, ***e***, ***i***; red), together with the anti-βIV-spectrin (***b***, ***f***, ***j***; green) and anti-parvalbumin (***c***, ***g***, ***k***; blue) antibodies. ***d***, ***h***, ***l***, Merged images. ***e–h***, Double arrowheads indicate examples of $Na_v1.1$-immunoreactive AISs of Purkinje cells. Scale bars, 50 μm. ***C***, Immunofluorescence histochemistry with the rabbit anti-C-terminal $Na_v1.1$ antibody (***a***, ***d***; red), together with the anti-phosphorylated neurofilament antibody mixture (SMI312) (***b***, ***e***; green). ***c***, ***f***, Merged images. Scale bars, 50 μm. IC, Inferior colliculus; CL, cerebellar lobule; M, molecular cell layer; P, Purkinje cell layer; G, granule cell layer.

These results suggest that $Na_v1.1$ is necessary to maintain but not initiate sustained fast spiking. This finding is consistent with decline of number of action potentials in dissociated hippocampal interneurons from heterozygous and homozygous $Na_v1.1$ knockout mice with increasing injected current recently reported by Yu et al. (2006). Moreover, resting membrane potential was more negative for *Gad1*$^{GFP/+}$:*Scn1a*$^{RX/+}$ interneurons (Fig. 8*C*) with a current–voltage relationship showing a significant rectification toward more negative voltages in *Gad1*$^{GFP/+}$:*Scn1a*$^{RX/+}$ interneurons (slope, $p = 0.0002$) (Fig. 8*D*). These results are in good agreement with reduced $Na_v1.1$ expression in *Gad1*$^{GFP/+}$:*Scn1a*$^{RX/+}$ interneurons. None of these differences were evident in neighboring pyramidal neurons (supplemental Fig. 9, available at www.jneurosci.org as supplemental material).

Because single-spike amplitude in *Gad1*$^{GFP/+}$:*Scn1a*$^{RX/+}$ interneurons was unaltered, other Na_v channels might be involved in action potential generation in the interneurons. Immunohistochemistry showed that $Na_v1.6$, which would be normally contained in neocortical AISs (Van Wart and Matthews, 2006), were localized at AISs of PV, fast-spiking interneurons in the developing neocortex (supplemental Fig. 10, available at www.jneurosci.org as supplemental material). In contrast to $Na_v1.1$, $Na_v1.6$ was also localized to AISs of the neocortical pyramidal cells.

Discussion

This study on mice genetically engineered to harbor a pathogenic SMEI mutation, R1407X, in the *Scn1a* gene, has advanced our understanding of how $Na_v1.1$ haploinsufficiency may cause epilepsy. Homozygous mice developed unstable gait and tonic-clonic, clonic, and polyspike-wave seizures in the second postnatal week. Heterozygous mice also showed epileptic recurrent seizure in the third postnatal week. Two abnormal phenotypes (namely, early onset with epileptic recurrent seizures in homozygous and heterozygous mice and unstable gait in homozygous mice) are analogous to the corresponding clinical features of SMEI. Thus, both homozygous and heterozygous mice should provide a useful tool for understanding the molecular basis of SMEI pathology and developing new therapeutic strategies for the treatment.

Homozygous mice were progressively malnourished from P10 and finally died before P20. Because the appearance of malnutrition was coincident with that of abnormal gait, nutritional starvation resulting from severely impaired locomotor activity seems to be one cause of premature death in the mice. In addition, moderately malnourished homozygous mice showed premature lethality, suggesting seizures and/or status epilepticus as other possible causes of premature death in the homozygous mice. Although heterozygous mice were not apparently malnourished, these heterozygous mice suffered sudden death after P18. At P18, they also developed recurrent seizures. Hence, seizures and/or status epilepticus might be the most probable cause of death in heterozygous mice. Interestingly, mortality rate in heterozygous mice varied with genetic background. The importance of genetic background, or modifier genes, has been also suggested in some familial SMEI cases in which SMEI patients have inherited the *SCN1A* mutations from mildly affected

parents (Gennaro et al., 2003; Nabbout et al., 2003; Meisler and Kearney, 2005; Yamakawa, 2005).

Truncated mutant $Na_v1.1$ protein was absent in knock-in mouse brains, indicating that the RX mutation inactivated the mutant allele in the brain, possibly because of the instability of either the *Scn1a* mRNA carrying a premature stop codon (Hentze and Kulozik, 1999) and/or truncated mutant $Na_v1.1$. Our findings are consistent with a recent report demonstrating that $Na_v1.1$-null mice also exhibited epileptic seizures (Yu et al., 2006), and we concluded that this $Na_v1.1$ haploinsufficiency caused the epileptic phenotypes in our knock-in mice. Although $Na_v1.1$ expression in SMEI patients' brains has never been assessed, we suggest that heterozygous nonsense and frame-shift SMEI mutations might inactivate the mutant alleles and lead to haploinsufficiency of $Na_v1.1$ (Sugawara et al., 2003; Meisler and Kearney, 2005; Mulley et al., 2005; Yamakawa, 2005) and therefore might parallel the current findings in our knock-in mice.

We previously reported a sporadic $Na_v1.2$ truncation mutation in a patient with intractable childhood epilepsy and severe mental decline and proposed a possible dominant-negative effect of truncated mutant $Na_v1.2$ on the electrophysiological properties of wild-type $Na_v1.2$ channels (Kamiya et al., 2004). In our knock-in mice, any modulating effects of the mutant truncated $Na_v1.1$ on wild-type $Na_v1.1$ and/or other sodium channel subunits can be excluded because only negligible levels of the mutant protein were expressed.

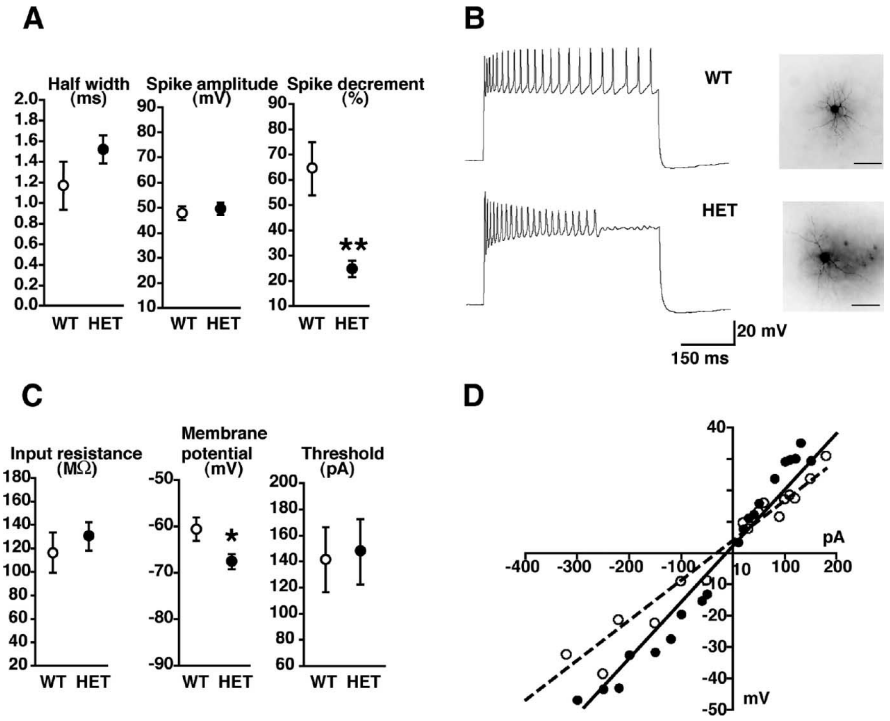

Figure 8. Summary of electrophysiological properties of $Gad1^{GFP/+}$:$Scn1a^{+/+}$ (WT; open circles; $n = 8$ neurons) and $Gad1^{GFP/+}$:$Scn1a^{RX/+}$ (HET; filled circles; $n = 8$ neurons) interneurons. ***A***, Properties (half-width and spike amplitude) of single action potentials at threshold and spike decrement of interneurons to a prolonged depolarizing current pulse (5× threshold; 500 ms). Spike decrement was calculated as percentage of last spike amplitude divided by first spike amplitude. Values represent means ± SEM; $^{**}p < 0.01$. ***B***, Representative traces of a WT (top) and HET (bottom) interneuron to a depolarizing current pulse at 5× threshold. Note that the rate of spike firing decreases mainly in HET interneurons. Representative biocytin-filled interneurons are shown for WT and HET mice. Scale bars, 50 μm. ***C***, Membrane properties of interneurons. Values represent means ± SEM; $^{*}p < 0.05$. ***D***, Plot of the current–voltage relationship of interneurons in WT (broken line) and HET (straight line) mice. Points represent voltages recorded at different injected current pulses. Linear regression is shown for each case.

In developing wild-type mouse brains, $Na_v1.1$ expression was significantly upregulated in the second and third postnatal weeks when abnormal phenotypes first appeared in homozygous and heterozygous mice. Although reduced $Na_v1.1$ expression apparently led to epileptic brains in our knock-in mice, neonates expressing $Na_v1.1$ at extremely low levels develop no spontaneous seizures, possibly because other α subunits, such as $Na_v1.2$ and $Na_v1.3$, might have compensatory effects in neonatal brains. During early development, the retina and caudal part of the brain switch from $Na_v1.2$ expression to $Na_v1.1$ expression (Beckh et al., 1989; Van Wart et al., 2005). Similarly, $Na_v1.3$ expression is high in fetal brains but becomes reduced after birth (Beckh et al., 1989). Unlike normal neonates, $Na_v1.2$ and $Na_v1.3$ probably do not fully compensate for loss of $Na_v1.1$ in our knock-in mice or in $Na_v1.1$-null mice (Yu et al., 2006).

Although previous immunohistochemical studies have indicated that $Na_v1.1$ is distributed homogenously in the brain (Westenbroek et al., 1989), our findings, which involve three different antibodies, suggest a heterogeneous distribution: $Na_v1.1$ expression in the caudal brain is higher than that in the rostral brain. Moreover, we verified the specificity of each antibody using the $Na_v1.1$-deficient homozygous knock-in mice as negative controls. Furthermore, our observations are supported by other studies, which used biochemical analysis (Gordon et al., 1987), Northern blot analysis (Beckh et al., 1989), and *in situ* hybridization [Furuyama et al., 1993; Black et al., 1994; the Allen brain atlas (www.brain-map.org)].

Our study has also revealed another interesting aspect of $Na_v1.1$ distribution. Although previous immunohistochemical analyses suggested that $Na_v1.1$ is generally localized to somata and dendrites of neurons (Westenbroek et al., 1989; Gong et al., 1999; Whitaker et al., 2001; Yu et al., 2006), our findings indicate that, with the exception of somata of hippocampal nonpyramidal cells, $Na_v1.1$ is generally localized to axons. Several other studies and data support this axonal $Na_v1.1$ localization. Recently, $Na_v1.1$ was reported to cluster predominantly to the AIS-like subsets of neuronal fibers in the developing retina (Van Wart et al., 2005) and AISs of retinal ganglion cells (Van Wart and Matthews, 2006; Van Wart et al., 2007). Moreover, $Na_v1.1$ possesses the motif required for localization to AISs (Garrido et al., 2003; Lemaillet et al., 2003; Pan et al., 2006).

In addition, although both hippocampal pyramidal and nonpyramidal cells express $Na_v1.1$ in somata (Westenbroek et al., 1989; Gong et al., 1999; Yu et al., 2006), our immunohistochemical analyses suggest that whereas $Na_v1.1$ is moderately expressed in somata of nonpyramidal cells, pyramidal cells expressed $Na_v1.1$ only at negligible levels. Our results are consistent with *in situ* hybridization data indicating that, in hippocampus, nonpyramidal cells express significantly higher $Na_v1.1$ levels than pyramidal cells [Furuyama et al., 1993; the Allen brain atlas (www.brain-map.org); this study]. Furthermore, our results may ex-

plain the interneuron-specific reduction in whole-cell sodium currents observed in hippocampus of $Na_v1.1$-null mice (Yu et al., 2006) (see Introduction). It will be interesting to conduct more detailed functional analyses of how the distinctive axonal distribution of $Na_v1.1$ contributes to its function and to abnormal phenotypes in mutant mice.

Most importantly, our immunohistochemistry revealed that $Na_v1.1$ is primarily localized to AISs, axons, and somata of PV interneurons in the developing neocortex and hippocampus. Also, the heterozygous fast-spiking interneurons that should be regarded as PV interneurons (Kawaguchi and Kondo, 2002) showed no shift in the single-spike amplitudes but rapidly decreased spike amplitudes in the spiking trains, suggesting that $Na_v1.1$ is involved in the maintenance but not in the initiation of sustained fast spiking in the interneurons and probably also in regulating GABA release from the interneurons.

Cortical PV interneurons are morphologically grouped as basket and chandelier cells whose axons exclusively innervate somata, proximal dendrites, and AISs of pyramidal cells (Somogyi et al., 1998; Kawaguchi and Kondo, 2002). Also, these interneurons are not only connected electrically and chemically to each other but are also self-innervated (Galarreta and Hestrin, 1999; Deans et al., 2001; Gibson et al., 2005; Bacci and Huguenard, 2006; Vida et al., 2006). We propose that lowered levels of functional $Na_v1.1$, arising from $Na_v1.1$ haploinsufficiency, alter function of the inhibitory local circuits and networks mediated by PV interneurons and, thereby, cause epileptic seizures.

Neocortical PV interneurons in Kv3.2 knock-out mice also show the rapid amplitude decrement in the spike trains (Lau et al., 2000). Kv3 channels are prominently expressed in PV interneurons in neocortex, and loss of Kv3.2 caused the decreased spike repolarization rate and reduced afterhyperpolarization currents, which may result in the amplitude decrement in the spike trains (Lau et al., 2000; Rudy and McBain, 2001). Moreover, Kv3.2 knock-out mice had increased seizure susceptibility, and some showed spontaneous epileptic seizures (Lau et al., 2000). It is therefore likely that impaired fast spiking in PV interneurons might contribute to seizure phenotypes in Kv3.2 knock-out and our $Na_v1.1$ knock-in mice.

SMEI mutant $Na_v1.1$ channels expressed heterologously in HEK293 cells are inactivated or have attenuated activity (Lossin et al., 2003; Sugawara et al., 2003; Rhodes et al., 2004; Ohmori et al., 2006). However, in HEK293 cells, whereas some GEFS+ and ICEGTC mutations cause loss-of-functional $Na_v1.1$ channels, other mutations are gain of functional (Lossin et al., 2002, 2003; Rhodes et al., 2005). These varying mutant channel properties indicate that coherent relationships between altered channel functions and clinical phenotypes are difficult to assess (George, 2005). The biophysical study on PV interneurons expressing GEFS+ and ICEGTC mutant $Na_v1.1$ channels may help to understand pathological differences among the disorders.

Cortical PV interneurons show correlated activity during theta oscillations and sharp-wave-associated ripples that have been implicated in information processing (Klausberger et al., 2003). Moreover, in the developing visual cortex, PV interneurons play important roles in critical period plasticity (Hensch, 2005a,b). It is likely that impaired fast spiking in PV interneurons might also contribute to slowed psychomotor development in the SMEI patients. Clearly, additional studies are required to understand the role of $Na_v1.1$ in maintaining PV circuits and in developing epileptic seizures, ataxia, and mental decline in SMEI patients. Finally, we cannot rule out the potential contribution to SMEI pathology of other Scn1a/$Na_v1.1$-expressing neurons.

References

Bacci A, Huguenard JR (2006) Enhancement of spike-timing precision by autaptic transmission in neocortical inhibitory interneurons. Neuron 49:119–130.

Beckh S, Noda M, Lubbert H, Numa S (1989) Differential regulation of three sodium channel messenger RNAs in the rat central nervous system during development. EMBO J 8:3611–3616.

Berghs S, Aggujaro D, Dirkx Jr R, Maksimova E, Stabach P, Hermel JM, Zhang JP, Philbrick W, Slepnev V, Ort T, Solimena M (2000) βIV spectrin, a new spectrin localized at axon initial segments and nodes of Ranvier in the central and peripheral nervous system. J Cell Biol 151:985–1002.

Bishop GA (1993) An analysis of HRP-filled basket cell axons in the cat's cerebellum. I. Morphometry and configuration. Anat Embryol (Berl) 188:287–297.

Black JA, Yokoyama S, Higashida H, Ransom BR, Waxman SG (1994) Sodium channel mRNAs I, II and III in the CNS: cell-specific expression. Brain Res Mol Brain Res 22:275–289.

Caldwell JH, Schaller KL, Lasher RS, Peles E, Levinson SR (2000) Sodium channel $Na_v1.6$ is localized at nodes of Ranvier, dendrites, and synapses. Proc Natl Acad Sci USA 97:5616–5620.

Catterall WA (2000) From ionic currents to molecular mechanisms: the structure and function of voltage-gated sodium channels. Neuron 26:13–25.

Claes L, Del-Favero J, Ceulemans B, Lagae L, Van Broeckhoven C, De Jonghe P (2001) De novo mutations in the sodium-channel gene *SCN1A* cause severe myoclonic epilepsy of infancy. Am J Hum Genet 68:1327–1332.

Deans MR, Gibson JR, Sellitto C, Connors BW, Paul DL (2001) Synchronous activity of inhibitory networks in neocortex requires electrical synapses containing connexin36. Neuron 31:477–485.

Escayg A, MacDonald BT, Meisler MH, Baulac S, Huberfeld G, An-Gourfinkel I, Brice A, LeGuern E, Moulard B, Chaigne D, Buresi C, Malafosse A (2000) Mutations of *SCN1A*, encoding a neuronal sodium channel, in two families with GEFS+2. Nat Genet 24:343–345.

Fujiwara T, Sugawara T, Mazaki-Miyazaki E, Takahashi Y, Fukushima K, Watanabe M, Hara K, Morikawa T, Yagi K, Yamakawa K, Inoue Y (2003) Mutations of sodium channel α subunit type 1 (SCN1A) in intractable childhood epilepsies with frequent generalized tonic-clonic seizures. Brain 126:531–546.

Fukuma G, Oguni H, Shirasaka Y, Watanabe K, Miyajima T, Yasumoto S, Ohfu M, Inoue T, Watanachai A, Kira R, Matsuo M, Muranaka H, Sofue F, Zhang B, Kaneko S, Mitsudome A, Hirose S (2004) Mutations of neuronal voltage-gated Na^+ channel α1 subunit gene *SCN1A* in core severe myoclonic epilepsy in infancy (SMEI) and in borderline SMEI (SMEB). Epilepsia 45:140–148.

Furuyama T, Morita Y, Inagaki S, Takagi H (1993) Distribution of I, II and III subtypes of voltage-sensitive Na^+ channel mRNA in the rat brain. Brain Res Mol Brain Res 17:169–173.

Galarreta M, Hestrin S (1999) A network of fast-spiking cells in the neocortex connected by electrical synapses. Nature 402:72–75.

Garrido JJ, Giraud P, Carlier E, Fernandes F, Moussif A, Fache MP, Debanne D, Dargent B (2003) A targeting motif involved in sodium channel clustering at the axonal initial segment. Science 300:2091–2094.

Gennaro E, Veggiotti P, Malacarne M, Madia F, Cecconi M, Cardinali S, Cassetti A, Cecconi I, Bertini E, Bianchi A, Gobbi G, Zara F (2003) Familial severe myoclonic epilepsy of infancy: truncation of $Na_v1.1$ and genetic heterogeneity. Epileptic Disord 5:21–25.

George Jr AL (2005) Inherited disorders of voltage-gated sodium channels. J Clin Invest 115:1990–1999.

Gibson JR, Beierlein M, Connors BW (2005) Functional properties of electrical synapses between inhibitory interneurons of neocortical layer 4. J Neurophysiol 93:467–480.

Gong B, Rhodes KJ, Bekele-Arcuri Z, Trimmer JS (1999) Type I and type II Na^+ channel α-subunit polypeptides exhibit distinct spatial and temporal patterning, and association with auxiliary subunits in rat brain. J Comp Neurol 412:342–352.

Gordon D, Merrick D, Auld V, Dunn R, Goldin AL, Davidson N, Catterall WA (1987) Tissue-specific expression of the R_I and R_{II} sodium channel subtypes. Proc Natl Acad Sci USA 84:8682–8686.

Hensch TK (2005a) Critical period plasticity in local cortical circuits. Nat Rev Neurosci 6:877–888.

Hensch TK (2005b) Critical period mechanisms in developing visual cortex. Curr Top Dev Biol 69:215–237.

Hentze MW, Kulozik AE (1999) A perfect message: RNA surveillance and nonsense-mediated decay. Cell 96:307–310.

Inda MC, Defelipe J, Munoz A (2006) Voltage-gated ion channels in the axon initial segment of human cortical pyramidal cells and their relationship with chandelier cells. Proc Natl Acad Sci USA 103:2920–2925.

Kalume FK, Yu FH, Catterall WA, Scheuer T (2005) Properties of sodium current in Purkinje neurons from Nav1.1 (−/−) mice: implications for resurgent current and ataxia. Soc Neurosci Abstr 31:151.10.

Kamiya K, Kaneda M, Sugawara T, Mazaki E, Okamura N, Montal M, Makita N, Tanaka M, Fukushima K, Fujiwara T, Inoue Y, Yamakawa K (2004) A nonsense mutation of the sodium channel gene *SCN2A* in a patient with intractable epilepsy and mental decline. J Neurosci 24:2690–2698.

Kawaguchi Y, Kondo S (2002) Parvalbumin, somatostatin and cholecystokinin as chemical markers for specific GABAergic interneuron types in the rat frontal cortex. J Neurocytol 31:277–287.

Klausberger T, Magill PJ, Marton LF, Roberts JD, Cobden PM, Buzsaki G, Somogyi P (2003) Brain-state- and cell-type-specific firing of hippocampal interneurons in vivo. Nature 421:844–848.

Komada M, Soriano P (2002) βIV-spectrin regulates sodium channel clustering through ankyrin-G at axon initial segments and nodes of Ranvier. J Cell Biol 156:337–348.

Krzemien DM, Schaller KL, Levinson SR, Caldwell JH (2000) Immunolocalization of sodium channel isoform NaCh6 in the nervous system. J Comp Neurol 420:70–83.

Lacas-Gervais S, Guo J, Strenzke N, Scarfone E, Kolpe M, Jahkel M, De Camilli P, Moser T, Rasband MN, Solimena M (2004) βIVΣ1 spectrin stabilizes the nodes of Ranvier and axon initial segments. J Cell Biol 166:983–990.

Lau D, Vega-Saenz de Miera EC, Contreras D, Ozaita A, Harvey M, Chow A, Noebels JL, Paylor R, Morgan JI, Leonard CS, Rudy B (2000) Impaired fast-spiking, suppressed cortical inhibition, and increased susceptibility to seizures in mice lacking Kv3.2 K^+ channel proteins. J Neurosci 20:9071–9085.

Lemaillet G, Walker B, Lambert S (2003) Identification of a conserved ankyrin-binding motif in the family of sodium channel alpha subunits. J Biol Chem 278:27333–27339.

Lossin C, Wang DW, Rhodes TH, Vanoye CG, George Jr AL (2002) Molecular basis of an inherited epilepsy. Neuron 34:877–884.

Lossin C, Rhodes TH, Desai RR, Vanoye CG, Wang D, Carniciu S, Devinsky O, George Jr AL (2003) Epilepsy-associated dysfunction in the voltage-gated neuronal sodium channel SCN1A. J Neurosci 23:11289–11295.

Meisler MH, Kearney JA (2005) Sodium channel mutations in epilepsy and other neurological disorders. J Clin Invest 115:2010–2017.

Mulley JC, Scheffer IE, Petrou S, Dibbens LM, Berkovic SF, Harkin LA (2005) SCN1A mutations and epilepsy. Hum Mutat 25:535–542.

Nabbout R, Gennaro E, Dalla Bernardina B, Dulac O, Madia F, Bertini E, Capovilla G, Chiron C, Cristofori G, Elia M, Fontana E, Gaggero R, Granata T, Guerrini R, Loi M, La Selva L, Lispi ML, Matricardi A, Romeo A, Tzolas V, et al. (2003) Spectrum of SCN1A mutations in severe myoclonic epilepsy of infancy. Neurology 60:1961–1967.

Ohmori I, Kahlig KM, Rhodes TH, Wang DW, George Jr AL (2006) Nonfunctional *SCN1A* is common in severe myoclonic epilepsy of infancy. Epilepsia 47:1636–1642.

Pan Z, Kao T, Horvath Z, Lemos J, Sul JY, Cranstoun SD, Bennett V, Scherer SS, Cooper EC (2006) A common ankyrin-G-based mechanism retains KCNQ and Na_V channels at electrically active domains of the axon. J Neurosci 26:2599–2613.

Rhodes TH, Lossin C, Vanoye CG, Wang DW, George Jr AL (2004) Noninactivating voltage-gated sodium channels in severe myoclonic epilepsy of infancy. Proc Natl Acad Sci USA 101:11147–11152.

Rhodes TH, Vanoye CG, Ohmori I, Ogiwara I, Yamakawa K, George Jr AL (2005) Sodium channel dysfunction in intractable childhood epilepsy with generalized tonic-clonic seizures. J Physiol (Lond) 569:433–445.

Rudy B, McBain CJ (2001) Kv3 channels: voltage-gated K^+ channels designed for high-frequency repetitive firing. Trends Neurosci 24:517–526.

Schauwecker PE (2002) Complications associated with genetic background effects in models of experimental epilepsy. Prog Brain Res 135:139–148.

Somogyi P, Támas G, Lujan R, Buhl EH (1998) Salient features of synaptic organisation in the cerebral cortex. Brain Res Brain Res Rev 26:113–135.

Sternberger LA, Sternberger NH (1983) Monoclonal antibodies distinguish phosphorylated and nonphosphorylated forms of neurofilaments in situ. Proc Natl Acad Sci USA 80:6126–6130.

Sugawara T, Mazaki-Miyazaki E, Fukushima K, Shimomura J, Fujiwara T, Hamano S, Inoue Y, Yamakawa K (2002) Frequent mutations of SCN1A in severe myoclonic epilepsy in infancy. Neurology 58:1122–1124.

Sugawara T, Tsurubuchi Y, Fujiwara T, Mazaki-Miyazaki E, Nagata K, Montal M, Inoue Y, Yamakawa K (2003) $Na_v1.1$ channels with mutations of severe myoclonic epilepsy in infancy display attenuated currents. Epilepsy Res 54:201–207.

Tamamaki N, Yanagawa Y, Tomioka R, Miyazaki J, Obata K, Kaneko T (2003) Green fluorescent protein expression and colocalization with calretinin, parvalbumin, and somatostatin in the GAD67-GFP knock-in mouse. J Comp Neurol 467:60–79.

Ulfig N, Nickel J, Bohl J (1998) Monoclonal antibodies SMI 311 and SMI 312 as tools to investigate the maturation of nerve cells and axonal patterns in human fetal brain. Cell Tissue Res 291:433–443.

Van Wart A, Matthews G (2006) Impaired firing and cell-specific compensation in neurons lacking $Na_v1.6$ sodium channels. J Neurosci 26:7172–7180.

Van Wart A, Boiko T, Trimmer JS, Matthews G (2005) Novel clustering of sodium channel $Na_v1.1$ with ankyrin-G and neurofascin at discrete sites in the inner plexiform layer of the retina. Mol Cell Neurosci 28:661–673.

Van Wart A, Trimmer JS, Matthews G (2007) Polarized distribution of ion channels within microdomains of the axon initial segment. J Comp Neurol 500:339–352.

Vida I, Bartos M, Jonas P (2006) Shunting inhibition improves robustness of gamma oscillations in hippocampal interneuron networks by homogenizing firing rates. Neuron 49:107–117.

Westenbroek RE, Merrick DK, Catterall WA (1989) Differential subcellular localization of the R_I and R_{II} Na^+ channel subtypes in central neurons. Neuron 3:695–704.

Whitaker WR, Faull RL, Waldvogel HJ, Plumpton CJ, Emson PC, Clare JJ (2001) Comparative distribution of voltage-gated sodium channel proteins in human brain. Brain Res Mol Brain Res 88:37–53.

Wong HK, Sakurai T, Oyama F, Kaneko K, Wada K, Miyazaki H, Kurosawa M, De Strooper B, Saftig P, Nukina N (2005) β Subunits of voltage-gated sodium channels are novel substrates of β-site amyloid precursor protein-cleaving enzyme (BACE1) and γ-secretase. J Biol Chem 280:23009–23017.

Yamakawa K (2005) Epilepsy and sodium channel gene mutations: gain or loss of function? NeuroReport 16:1–3.

Yu FH, Mantegazza M, Westenbroek RE, Robbins CA, Kalume F, Burton KA, Spain WJ, McKnight GS, Scheuer T, Catterall WA (2006) Reduced sodium current in GABAergic interneurons in a mouse model of severe myoclonic epilepsy in infancy. Nat Neurosci 9:1142–1149.